

A comparison of nonlinear filtering methods for blackbody radiation applications in photonics

Isaac Spotts ^a, C. Harrison Brodie ^b, S. Andrew Gadsden ^b, Mohmmad Al-Shabi ^c, and Christopher M. Collier ^{ab}

^a School of Engineering, University of British Columbia Okanagan Campus, 3333 University Way, Kelowna, BC, Canada; ^b School of Engineering, University of Guelph, 50 Stone Road East, Guelph, ON, Canada; ^c Department of Mechanical and Nuclear Engineering, University of Sharjah, Sharjah, United Arab Emirates

ABSTRACT

Kalman filtering (KF) is a widely used filtering technique in highly predictable temporal-mechanical systems where system noise can be modelled with a gaussian function. Improving the signal quality during acquisition is conventionally accomplished by increasing integration time in acquisition. However, this increases the signal acquisition time in photonic systems. In high noise applications, acquisition time is low, and this post-process filtering technique can be applied to increase signal quality. This work explores the comparison of the KF, and nonlinear filtering methods to a simulated blackbody radiation signal where gaussian noise is added to mimic electrical interference. Three filters are selected for comparison on the ability to improve the root mean square error (RMSE) of a simulated measured signal with respect to a simulated actual signal. The filters that are compared in this work are the Extended Kalman Filter (EKF), the Unscented Kalman (UKF), and the Extended Sliding Innovation Filter (ESIF). The filters use a calibration temperature that the filter model uses to determine expected values. To compare the filters, the RMSE is evaluated when error is introduced to the simulation by changing the actual temperature to values equal, below, and above the calibration temperature. Two additional scenarios were considered to test filter robustness. The first scenario uses changes in model temperature occurring as a function of wavelength (i.e., temperature change mid-scan). The second scenario introduces impurities with different emission values. The ESIF demonstrated favorable performance over the other considered filters, showing promise in optical applications.

Keywords: Signal processing, Kalman filter, Blackbody radiation, Nonlinear filtering, Spectroscopy.

1. INTRODUCTION

Estimation theory is a field of statistical analysis that involves estimating the true value of measured data with a random component¹. Sensors that are susceptible to measurements with random noise can leverage methods of estimation theory to improve signal quality¹. The behaviour of unstructured noise can be modelled as a Gaussian distribution with a mean of zero². Using Estimation theory techniques, a filter can be designed to lower unstructured random noise produced by photonic emitters. The effectiveness of this filter is dependent on how well the true value of measured system can be predicted. A well-established estimation theory filter that generates an optimal gain in linear systems to reduce gaussian noise of a system, is the Kalman filter (KF)³. The design of a filter that can remove noise is beneficial to photonic sensors that perform poorly due to increased noise (e.g., low integration time spectroscopy)^{4,5}. Extended works of the KF have also been created for non-linear system using a non-ideal solution of the model⁶.

The unscented Kalman filter and extended Kalman filter (UKF, and EKF respectively) are generally used as alternatives to the Kalman filter when filtering nonlinear systems⁷. In the applications described above the KF-based methods are derived with precise restrictions⁷. The restrictions on KF-based systems are that the system and measurements can be accurately modeled, and that the system and measurement noise is random and equal at all frequencies⁸. When these assumptions are invalid then the filter results provided by the KF may not accurately represent the true state values. A solution to robustness issues in KF is a new filter named the sliding innovation filter (SIF)⁹. Using a switching gain to provide estimates that are close to true state trajectories, the SIF is designed based on sliding mode theory⁹. This solution provides a sub-optimal solution to the system and measurement estimates to increase robustness when modelling disturbances and uncertainties.

Recently photonic systems have begun leveraging the KF for improvement to system signal-to-noise ratio (SNR) in high noise systems^{10,11}. In optics, Kalman filter techniques are applied in light emitting diode data transfer using EKF based alignment, reduction of time delay in spatial tracking through light emitting diode infrastructure, and parameter estimation in optical tomography applications¹²⁻¹⁴. The spectral analysis of blackbody radiators is a photonic system that follows satisfies most of the assumptions that are ideal for KF implementation. In this work the EKF, UKF and a new sliding innovation filter technique are applied to a simulation of a spectral analysis emitted by a blackbody radiator, for comparison in the estimation of a true value given a measured system. This comparison could provide insight on the appropriate filter for a potential application in noisy photonic systems such as spectroscopy with low integration time requirements.

2. ESTIMATION OF NONLINEAR PHOTONIC SYSTEMS

Blackbody radiators follow a well-established model that is described by Planck's Law,

$$A(\lambda, T) = \frac{2hc^2}{\lambda^5} \left(\frac{1}{e^{\frac{hc}{\lambda kT}} - 1} \right), \quad (1)$$

where the blackbody radiator temperature is T , the speed of light inside a vacuum is c , Plank's constant is represented by h , k is Boltzmann's constant, and the electromagnetic wavelength is represented by λ . To develop a filter model a temperature must be selected for completion of equation (1), this temperature will be referred to as the model temperature. Considering Planck's Law is a non-linear system, the KF will be unable to provide a perfect solution to the optimal gain for identifying the true value of the measured system.

2.1 The Extended Kalman Filter

The first extension of KF to non-linear systems is the EKF. Equations (2) and (3) describe a non-linear system f and measurement functions h .

$$x_{k+1} = f(x_k, u_k) + w_k \quad (2)$$

$$z_{k+1} = h(x_{k+1}) + v_{k+1} \quad (3)$$

In these equations x_k is a reference to a given state at time k , the system input is represented by u_k , system noise is represented by w_k , the measurement is represented by z_k , the measurement noise is represented v_k . To mimic electronic noise that can be found in spectrometers the measurement and system noise are selected to be gaussian noise.

To produce the model for the EKF, Jacobian matrices are calculated (First-order Taylor series approximations), which linearizes the non-linearities within the system. Equations (4) and (5) apply linearization to the nonlinear system and measurement functions, respectively.

$$F_{k+1} = \left. \frac{\partial f}{\partial x} \right|_{\hat{x}_{k|k}, u_k} \quad (4)$$

$$H_{k+1} = \left. \frac{\partial h}{\partial x} \right|_{\hat{x}_{k+1|k}} \quad (5)$$

The objective of all estimators (e.g., EKF, UKF, SIF) is to calculate the true state value x_{k+1} . Elevated noise has been injected into the model through the simulated measurements z_{k+1} . The goal of the estimators in this application is to retrieve the true value of the intensity at a given wavelength λ , and reduce the injected noise in the measurement. The EKF is defined as an estimator that uses a predictor-corrector strategy. In the prediction stage, the state estimates, state error covariance (the amount of error in the estimation process), and calculation of the innovation (error in the measurement), are predicted as described by (6), (7), and (8), respectively.

$$\hat{x}_{k+1|k} = f(\hat{x}_{k|k}, u_k) \quad (6)$$

$$P_{k+1|k} = F_{k+1} P_{k|k} F_{k+1}^T + Q_{k+1} \quad (7)$$

$$\tilde{z}_{k+1|k} = z_{k+1} - h(\hat{x}_{k+1|k}) \quad (8)$$

The system noise covariance matrix is represented by Q , where the subscript $k + 1|k$ represents a priori (“before the fact”) information (found in the prediction stage). During the update stage an EKF gain is calculated using (9), updating the estimates found in (10), and the state error covariance matrix seen in (11).

$$K_{k+1} = H_{k+1}P_{k+1|k}^T(H_{k+1}P_{k+1|k}H_{k+1}^T + R_{k+1})^{-1} \quad (9)$$

$$\hat{x}_{k+1|k+1} = \hat{x}_{k+1|k} + K_{k+1}\tilde{z}_{k+1|k} \quad (10)$$

$$P_{k+1|k+1} = (I - K_{k+1}H_{k+1})P_{k+1|k}(I - K_{k+1}H_{k+1})^T + K_{k+1}R_{k+1}K_{k+1}^T \quad (11)$$

In these equations, the measurement noise covariance matrix is represented by R_k , and an identity matrix (represented by I) with dimensions $n \times n$ given that n is the number of states. The (“after the fact”) information is represented by the posteriori subscript $k + 1|k + 1$. Equations (4) through (11) represent the estimation process of the EKF. The EKF is used for the systems and measurements that are modelled in (2) and (3). At each time step, the predictor-corrector method is repeated through iteration.

2.2 The Unscented Kalman Filter

Another type of filter that is designed for treatment of non-linear systems based on the design of the KF, is the UKF. Unlike the EKF, the UKF does not use First-Order approximations of non-linear systems. Instead, the UKF uses sigma points to approximate the nonlinearities in the system. The UKF also uses a predictor-corrector strategy for the treatment of data. The first step is the generation of $2n + 1$ sample points which are referred to as sigma points. The n state system will be approximated by the sigma points that are generated. The sigma point that is generated initially, with its corresponding weight are defined in (12) and (13), respectively.

$$X_{0,k|k} = \hat{x}_{k|k} \quad (12)$$

$$W_0 = \frac{\kappa}{n + \kappa} \quad (13)$$

In equation (13) K is a reference to a design parameter that is typically chosen to be less than 1. The corresponding weights of the remainder ($2n$) of the sigma points is defined respectively as:

$$X_{i,k|k} = \hat{x}_{k|k} \pm \left(\sqrt{(n + \kappa)P_{k|k}} \right)_i \quad (14)$$

$$W_i = \frac{1}{[2(n + \kappa)]} \quad (15)$$

Where subscript i is a reference to the i^{th} sigma point. The subscript of the square root i in (14) refers to the i^{th} column or row of the matrix square root result. The second step in the predictor-corrector strategy is the prediction of state estimates and covariance. To propagate the sigma points through the model equation (16) is used, the predicted state estimates are then calculated by the resulting weights from (15).

$$\hat{X}_{i,k+1|k} = f(X_{i,k|k}, u_k) \quad (16)$$

$$\hat{x}_{k+1|k} = \sum_{i=0}^{2n} W_i \hat{X}_{i,k+1|k} \quad (17)$$

The state error covariance matrix is then calculated from the values found in (16) and (17), which is described in (18).

$$P_{k+1|k} = \sum_{i=0}^{2n} W_i (\hat{X}_{i,k+1|k} - \hat{x}_{k+1|k})(\hat{X}_{i,k+1|k} - \hat{x}_{k+1|k})^T + Q_k \quad (18)$$

In the third step, the measurement covariance, and measurement are calculated. To propagate the sigma points through the nonlinear measurement model (19) is used. Additionally, the measurement is predicted using (20).

$$\hat{Z}_{i,k+1|k} = h(\hat{X}_{i,k+1|k}, u_k) \quad (19)$$

$$\hat{z}_{k+1|k} = \sum_{i=0}^{2n} W_i \hat{Z}_{i,k+1|k} \quad (20)$$

Using (19) and (20), the measurement covariance can be calculated as follows:

$$P_{zz,k+1|k} = \sum_{i=0}^{2n} W_i (\hat{Z}_{i,k+1|k} - \hat{z}_{k+1|k}) (\hat{Z}_{i,k+1|k} - \hat{z}_{k+1|k})^T + R_{k+1} \quad (21)$$

The fourth step is the calculation of the cross-covariance using (22) in conjunction (21) to calculate the UKF gain.

$$P_{xz,k+1|k} = \sum_{i=0}^{2n} W_i (\hat{X}_{i,k+1|k} - \hat{x}_{k+1|k}) (\hat{Z}_{i,k+1|k} - \hat{z}_{k+1|k})^T \quad (22)$$

$$K_{k+1} = P_{xz,k+1|k} P_{zz,k+1|k}^{-1} \quad (23)$$

The final step of the predictor-corrector strategy for the UKF is the calculation of updated state estimates as shown in (24) and the updated state error covariance matrix shown in (25).

$$\hat{x}_{k+1|k+1} = \hat{x}_{k+1|k} + K_{k+1} (z_{k+1} - \hat{z}_{k+1|k}) \quad (24)$$

$$P_{k+1|k+1} = P_{k+1|k} - K_{k+1} P_{zz,k+1|k} K_{k+1}^T \quad (25)$$

The predictor-corrector strategy of the UKF is described through equations (12) to (25), which is completed iteratively. The UKF is more mathematically complex than the EKF, however it does not sacrifice accuracy of the system model due to linearization.

2.3 The Sliding Innovation Filter and Extended Sliding Innovation Filter

A similar filter that uses the predictor-corrector based filter method is the SIF, and the non-linear form, the extending sliding innovation filter (ESIF). The ESIF differs from the KF-based methods by using a sliding mode technique to treat data. Using the ESIF will produce a sub-optimal result for linear systems, however, when used to treat non-linear systems it is more robust than the KF. The calculations performed in the ESIF are similar to the EKF which are shown in equations (2) to (11). The ESIF differs from the EKF in the calculation of the gain, where the ESIF gain is calculated using (26).

$$K_{k+1} = H_{k+1}^+ \overline{\text{sat}}(|\check{z}_{k+1|k}|/\delta) \quad (26)$$

In this equation the pseudoinverse is represented by $+$, the diagonal matrix elements equal to saturated values is represented by $\overline{\text{sat}}$, the absolute innovation or measurement error is represented by $|\check{z}_{k+1|k}|$, and the tunable sliding boundary layer parameter is represented by δ . This sliding boundary layer is often identified through optimization of the filter parameter δ . Common techniques that are applied to optimize this parameter are trial and error, or grid search techniques.

3. SIMULATION PARAMETERS

The wavelength spacing in all simulations conducted is 10 nm ($d\lambda = 10$ nm). The simulations were performed over the interval of $\lambda = 200$ nm to $\lambda = 3400$ nm. The first filter that is used to treat the data from the simulation is the EKF. Following equation (1) the first state (x) of the model is the intensity as a function of wavelength. Taking the derivative of (1) provides the second state (\dot{x}), which can be seen as $\alpha - \beta$ in (27) and described further in equations (28) and (29).

$$x_{k+1} = \begin{vmatrix} 1 & d\lambda \\ 0 & \alpha - \beta \end{vmatrix} x_k + w_k \quad (27)$$

$$\alpha = \frac{2h^3 c^3 e^{hc/\lambda kT}}{kT\lambda^7} \left(\frac{1}{e^{hc/\lambda kT} - 1} \right)^2 \quad (28)$$

$$\beta = \left(\frac{10 c^2 h}{\left(e^{hc/\lambda kT} - 1 \right) \lambda^6} \right) \quad (29)$$

Where,

$$w = \sim|Q| \quad (30)$$

and Q , the model system covariance parameter is defined in (31).

$$Q = \begin{vmatrix} 10^{-2} & 0 \\ 0 & 10^{-2} \end{vmatrix} \quad (31)$$

The second filter used to treat the data from the simulation is the UKF. The model of the UKF for the predictor-corrector strategy, is described in (32).

$$x_{k+1} = \begin{vmatrix} 1 & d\lambda(\dot{x}) \\ 0 & \alpha - \beta \end{vmatrix} x_k + w_k. \quad (32)$$

The final filter used to treat the data from the simulation is the ESIF. The ESIF uses a tunable parameter, the sliding boundary layer δ . The value for δ was found through an iterative process that tracked the root mean squared error (RMSE) between the true state value and the treated data. To ensure that overfitting to one scenario did not occur the same δ was used for all scenarios, which can be seen in (33).

$$\delta = \begin{vmatrix} 4 \times 10^{13} & 0 \\ 0 & 1 \times 10^2 \end{vmatrix} \quad (33)$$

To simulate the system, a model of both the first state and second state was developed using the theoretical model for blackbody radiation which is provided in (1). The matrix of this model is shown in (34).

$$z_{k+1} = \begin{vmatrix} \frac{2hc^2}{\lambda^5} \left(\frac{1}{e^{\frac{hc}{\lambda kT}} - 1} \right) & 0 \\ 0 & \alpha - \beta \end{vmatrix} z_k + v_k \quad (34)$$

Random gaussian noise is represented by v . The magnitude of this noise was chosen to scale proportionally to the intensity at an arbitrary wavelength ($\lambda = 690$ nm), which is shown in (35).

$$v \sim \left| R \times \frac{10x_{690 \text{ nm}}}{7} \right| \quad (35)$$

In this equation R represents the measurement noise covariance, which is shown in (36).

$$R = \begin{vmatrix} 25 & 0 \\ 0 & 25 \end{vmatrix} \quad (36)$$

This matrix is dependent on the noise in the system. This value can either decrease or increase depending on if the simulation is of a low noise or high noise system, respectively.

4. SIMULATION RESULTS

In section 3, three non-linear filters were described, the EKF, UKF and the ESIF. These filters are implemented on a simulated data set for a comparison in how effective each filter performs in reducing noise. The quantification of this performance is evaluated using two metrics, RMSE and predicted temperature. The RMSE is calculated by using the

treated data set and the true state values. The predicted temperature is identified through curve fitting spectrums generated by equation (1) to determine the most accurate wavelength spectrum that matches the treated data set.

Table 1. The results (predicted temperature and percent RMSE reduction) from each of the simulated scenarios, (below model temperature, model temperature, above model temperature, change in temperature mid scan, and absorption lines) for each filter (EKF, UKF, and ESIF) tabulated.

Filter		1: Below model temperature T = 5000K	2: Model temperature T = 5500K	3: Above model temperature T = 6000K	4: Change in temperature, mid scan T = 5500 to 6000K		5: Absorption lines T = 5500K
EKF	Predicted T value(s) (K)	4980	5450	5890	5450	5450	N/A
	RMSE reduction (%)	78.4	55.5	-1.0	-6.17		31.0
UKF	Predicted T value(s) (K)	4970	5530	6040	5500	6010	N/A
	RMSE reduction (%)	39.1	68.0	43.3	55.0		44.4
ESIF	Predicted T value(s) (K)	5020	5530	6020	5500	6000	N/A
	RMSE reduction (%)	79.5	74.2	62.7	55.4		44.8

Five separate simulations are generated that provide different scenarios for the filters to be evaluated. Scenario one generates a spectrum for a temperature that is 500 K ($T = 5000$ K) below the filter model temperature ($T = 5500$ K). Scenario two generates a spectrum for a temperature that is at the filter model temperature ($T = 5500$ K). Scenario three generates a spectrum for a temperature that is 500 K ($T = 6000$ K) above the filter model temperature ($T = 5500$ K). Scenario four generates a spectrum that changes in temperature during the scan where the initial temperature is the filter model temperature ($T = 5500$ K), and the changed temperature is 500 K above the filter model temperature ($T = 6000$ K). The performance of each filter in terms of predicted temperature and percent RMSE is tabulated in table 1.

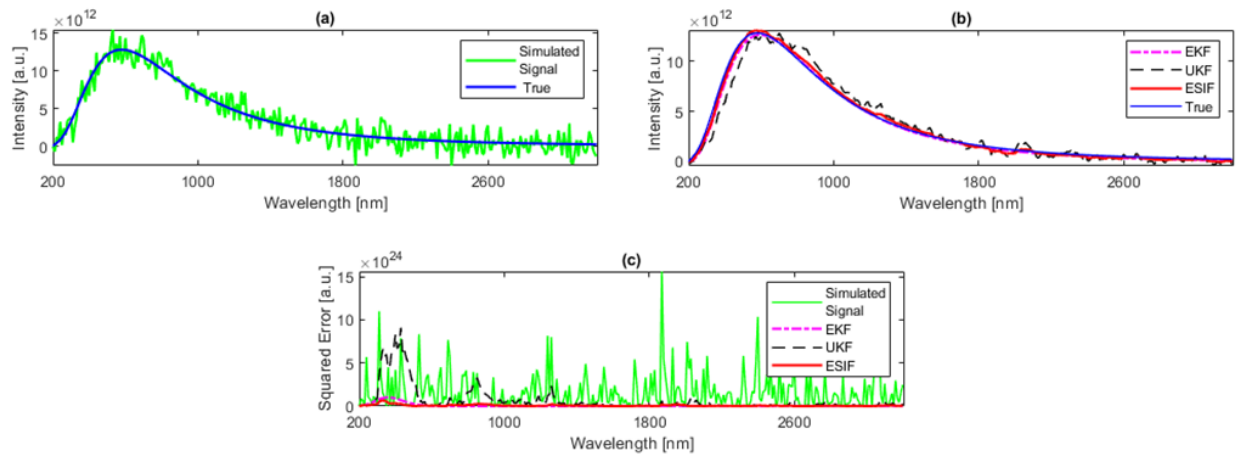


Figure 1. Results of scenario one ($\Delta T = -500$ K) displayed graphically. In (a) a spectrum is produced using the Stephen-Boltzmann equation at a temperature of 5000 K (true), overlaid with the simulated measurement (simulated signal), which includes the injected noise. The graph in (b) depicts the true data set overlaid with the intensity measurement data of each corresponding filter (EKF, UKF, and ESIF) treatment. The graph in (c) depicts the squared error of the simulated

measurement, and the simulated measurement after treatment with each corresponding filter, in reference to the true data set.

In Figure 1 the results from scenario one are displayed. In this scenario the simulated generated spectrum is 500 K below the filter model temperature ($T = 5000$ K and $T = 5500$ K, respectively). The simulated measurements that would be generated from a spectrometer are seen in fig. 1(a). In fig. 1(b). Each filter demonstrates the ability to reasonably track the generated spectrum with these parameters, while reducing the noise injected into the system. The EKF and ESIF demonstrate an advantage over the UKF when tracking generated spectrums that are lower than the filter model temperature. The reduction in RMSE due to the filters is demonstrated in fig. 1(c) where the RMSE is plotted with respect to wavelength. When predicting the temperature, the EKF and the ESIF provide the results ($T = 4980$ K and $T = 5020$ K, respectively) closest to the true measurement model temperature ($\Delta T = 20$ K).

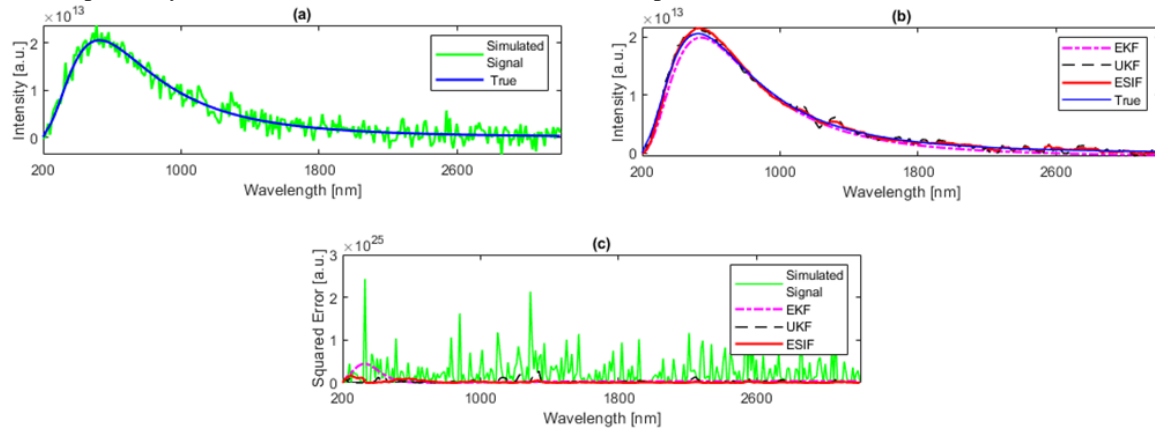


Figure 2. Results of scenario two ($\Delta T = 0$ K) displayed graphically. In (a) a spectrum is produced using the Stephen-Boltzmann equation at a temperature of 5500 K (true), overlaid with the simulated measurement (simulated signal), which includes the injected noise. The graph in (b) depicts the true data set overlaid with the intensity measurement data of each corresponding filter (EKF, UKF, and ESIF) treatment. The graph in (c) depicts the squared error of the simulated measurement, and the simulated measurement after treatment with each corresponding filter, in reference to the true data set.

In Figure 2 the results from scenario two are displayed. In this scenario the simulated generated spectrum at the filter model temperature ($T = 5500$ K). The simulated measurements that would be generated from a spectrometer are seen in fig. 2(a). In fig. 2(b). Each filter demonstrates the ability to reasonably track the generated spectrum with these parameters, while reducing the noise injected into the system. The ESIF demonstrate an advantage over both the UKF and EKF when tracking generated spectrums that are equal to the filter model temperature. The reduction in RMSE due to the filters is demonstrated in fig. 2(c) where the RMSE is plotted with respect to wavelength. When predicting the temperature, the EKF and the ESIF provide the results ($T = 5530$ K) closest to the true measurement model temperature ($\Delta T = 30$ K).

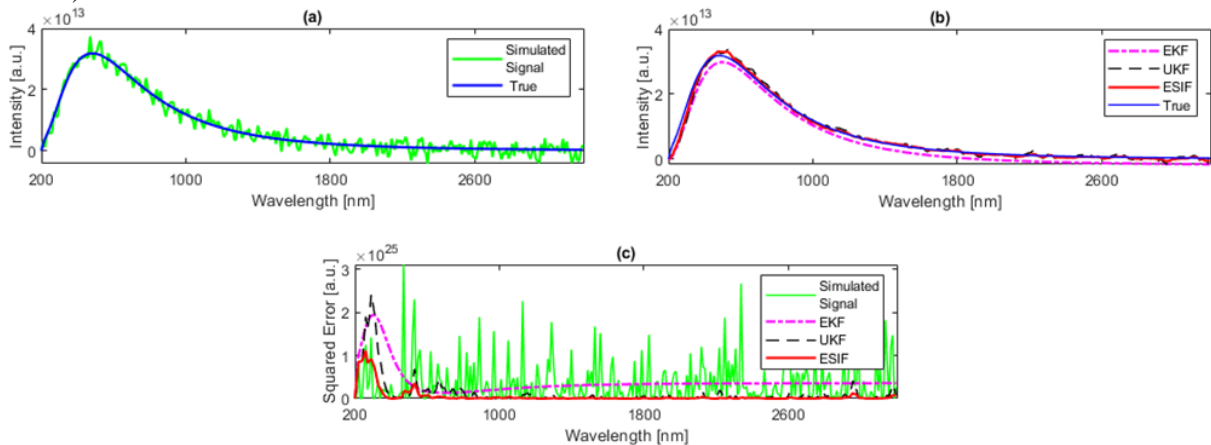


Figure 3. Results of scenario three ($\Delta T = 500$ K) displayed graphically. In (a) a spectrum is produced using the Stephen-Boltzmann equation at a temperature of 6000 K (true), overlaid with the simulated measurement (simulated signal), which

includes the injected noise. The graph in (b) depicts the true data set overlaid with the intensity measurement data of each corresponding filter (EKF, UKF, and ESIF) treatment. The graph in (c) depicts the squared error of the simulated measurement, and the simulated measurement after treatment with each corresponding filter, in reference to the true data set.

In Figure 3 the results from scenario three are displayed. In this scenario the simulated generated spectrum is 500 K above the filter model temperature ($T = 6000$ K and $T = 5500$ K, respectively). The simulated measurements that would be generated from a spectrometer are seen in fig. 3(a). In fig. 3(b). The UKF and the ESIF demonstrate the ability to reasonably track the generated spectrum, while reduce the RMSE from the noise injected into the system. The EKF is unable to adequately track the generated spectrum and increases the RMSE from the noise injected into the system. The reduction in RMSE due to the UKF and ESIF is demonstrated in fig.3(c) where the RMSE is plotted with respect to wavelength. The UKF and ESIF demonstrate an advantage over the EKF when tracking generated spectrums that are above than the filter model temperature. When predicting the temperature, the ESIF provides the results ($T = 6020$ K) closest to the true measurement model temperature ($\Delta T = 20$ K).

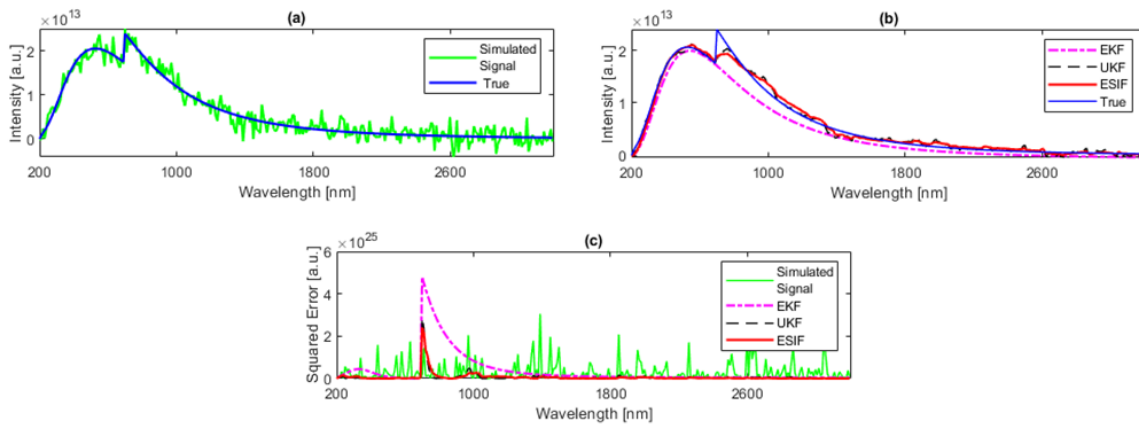


Figure 4. Results of scenario four (change in temperature at $\lambda = 500$ nm ($\Delta T = 0$ K to $\Delta T = 500$ K)) displayed graphically. In (a) a spectrum is produced using the Stephen-Boltzmann equation at a temperature of 5500 K, and 6000 K (true), overlaid with the simulated measurement (simulated signal), which includes the injected noise. The graph in (b) depicts the true data set overlaid with the intensity measurement data of each corresponding filter (EKF, UKF, and ESIF) treatment. The graph in (c) depicts the squared error of the simulated measurement, and the simulated measurement after treatment with each corresponding filter, in reference to the true data set.

In Figure 4 the results from scenario four are displayed. In this scenario the generated spectrum has a 500 K temperature change (from $T = 5500$ K to $T = 6000$ K) occur at $\lambda = 500$ nm. The simulated measurements that would be generated from a spectrometer are seen in fig. 4(a). In fig. 4(b). The UKF and the ESIF demonstrate the ability to reasonably track the generated spectrum, including the spectrum shift from the change in temperature, while reduce the RMSE from the noise injected into the system. The EKF is unable to adequately track the spectrum shift caused by the temperature change and increases the RMSE from the noise injected into the system. The UKF and ESIF demonstrate an advantage over the EKF when tracking changes within the system spectrums. When predicting the temperature, the ESIF provides the results ($T = 5500$, and $T = 6000$ K) closest to the true measurement model temperature ($\Delta T = 0$ K, and $\Delta T = 0$ K respectively).

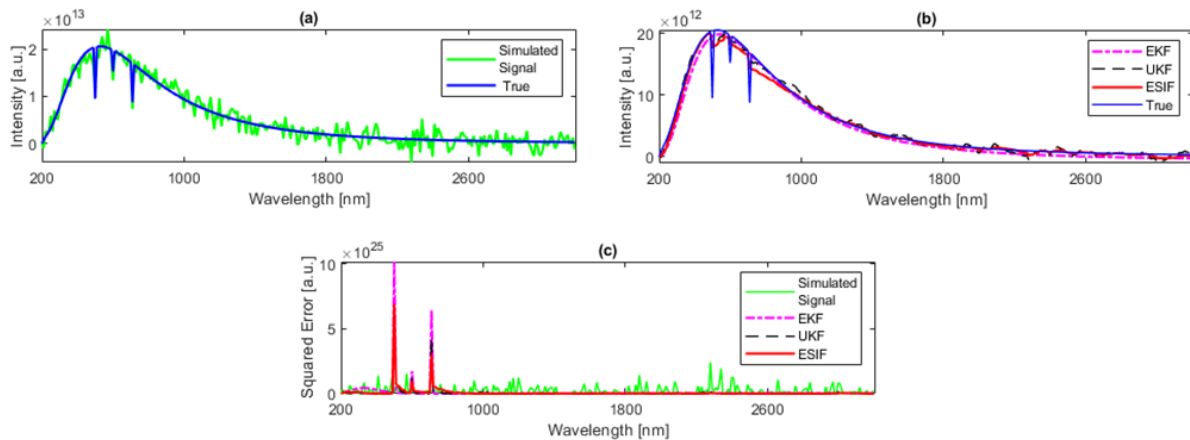


Figure 5. Results of scenario five (absorption lines at $\lambda = 300$ nm, $\lambda = 400$ nm, and $\lambda = 510$ nm) displayed graphically. In (a) a spectrum is produced using the Stephen-Boltzmann equation at a temperature of 5500 K (true), overlaid with the simulated measurement (simulated signal), which includes the injected noise. The graph in (b) depicts the true data set overlaid with the intensity measurement data of each corresponding filter (EKF, UKF, and ESIF) treatment. The graph in (c) depicts the squared error of the simulated measurement, and the simulated measurement after treatment with each corresponding filter, in reference to the true data set.

In Figure 5 the results from scenario four are displayed. In this scenario contaminants to the system have been modeled through the introduction of absorption lines at specific wavelengths ($\lambda = 300$ nm, $\lambda = 400$ nm, $\lambda = 510$ nm). The simulated measurements that would be generated from a blackbody emitter with characteristics of contaminants in a blackbody spectrum are seen in fig. 5(a). In fig. 5(b). The EKF demonstrates an inability to track the simulated spectral lines caused by the contaminants. In fig. 5(b) it is shown for the EKF, there is no change from the filter model in the treated state values after each contaminant spectral line is introduced. In fig. 5(c) it is shown that the UKF and ESIF have an increased error when each contaminant spectral line occurs. However, unlike the EKF, the UKF and ESIF manage to identify the change in the system.

5. CONCLUDING REMARKS

Three filters (EKF, UKF, and ESIF) are presented to treat a noise injected simulated spectrum calculated using the Planck's Law. To compare the presented filters, five scenarios were developed where unique responses are considered. In these scenarios it is shown that the EKF is unable to adequately filter above filter model temperature (scenario three), and changes that occur in the measurement model (scenarios four, and five). The UKF both demonstrated the ability to reduce RMSE in all scenarios and were able to track changes that occurred in the measurement model. The ESIF is the highest performing filter given the metrics used in the analysis conducted in this research (RMSE reduction and predicted temperature). Therefore, the use of ESIF in high noise photonic applications such as low-integration time spectroscopy for blackbody radiators would be advantageous.

REFERENCES

- [1] Peesapati, R., Sabat, S. L., Karthik, K. P., Nayak, J. and Giribabu, N., "Efficient hybrid Kalman filter for denoising fiber optic gyroscope signal," *Optik (Stuttg)*. **124**(20), 4549–4556 (2013).
- [2] Jáuregui Misas, C., López-Higuera, J. M. and López-Amo, M., "Adaptive filters applied to the interrogation of photonic sensors," *IEEE Sens. J.* **6**(3), 748–753 (2006).
- [3] Chen, S. Y., Wang, Y., Wu, C. C., Liu, C. and Chang, C. I., "Real-time causal processing of anomaly detection for hyperspectral imagery," *IEEE Trans. Aerosp. Electron. Syst.* **50**(2), 1511–1534 (2014).
- [4] Harrison Brodie, C. and Collier, C. M., "Single-point detection architecture via liquid crystal modulation for

- hyperspectral imaging systems,” *IEEE Access* **8**, 185012–185020 (2020).
- [5] Wang, S., Chang, C., Jensen, J. L. and Jensen, J. O., “Spectral abundance fraction estimation of materials using Kalman filters,” *Chem. Biol. Standoff Detect. II* **5584**, J. O. Jensen and J.-M. Theriault, Eds., 210–220, SPIE (2004).
- [6] Gadsden, A., Habibi, S., Dunne, D. and Kirubarajan, T., “Nonlinear estimation techniques applied on target tracking problems,” *J. Dyn. Syst. Meas. Control. Trans. ASME* **134**(5) (2012).
- [7] Gadsden, S. A., “Smooth Variable Structure Filtering: Theory and Applications” (2011).
- [8] Cinar, R. F., Kocadag, F. and Demirkol, A., “Kalman filter aided target density function for radar imaging,” *J. Eng.* **2019**(19), 5602–5604 (2019).
- [9] Gadsden, S. and AlShabi, M., “The Sliding Innovation Filter,” *IEEE Access* **8**, 1 (2020).
- [10] Riggs, A. J. E., Kasdin, N. J. and Groff, T. D., “Recursive starlight and bias estimation for high-contrast imaging with an extended Kalman filter,” *J. Astron. Telesc. Instruments, Syst.* **2**(1), 011017 (2016).
- [11] Shen, Y., Lou, S. and Wang, X., “Estimation method of point spread function based on Kalman Filter for accurately evaluating real optical properties of photonic crystal fibers,” *Appl. Opt.* **53**(9), 1838 (2014).
- [12] Hossan, M. T., Chowdhury, M. Z., Islam, A. and Jang, Y. M., “A Novel Indoor Mobile Localization System Based on Optical Camera Communication,” *Wirel. Commun. Mob. Comput.* **2018** (2018).
- [13] Baez, G. R., Pomarico, J. A. and Elicabe, G. E., “An improved extended Kalman filter for diffuse optical tomography,” *Biomed. Phys. Eng. Express* **3**(1), 015013 (2017).
- [14] Solanki, P. B. and Tan, X., “Extended Kalman Filter-Based 3D Active-Alignment Control for LED Communication,” *Proc. - IEEE Int. Conf. Robot. Autom.* **23**(4), 4881–4888 (2018).